A FULLY 3D UNAVERAGED NON-LOCALISED ELECTRON, PARALLELIZED-COMPUTATIONAL MODEL OF THE FEL

L.T. Campbell, R. Martin and B.W.J. McNeil
SUPA, Department of Physics, University of Strathclyde, Glasgow, UK

Abstract

A new unaveraged 3D parallelized numerical model has been developed that will allow investigation of previously unexplored FEL physics. Unaveraged models are required to describe such effects as amplification of Coherent Spontaneous Emission and non-localised electron dynamics (see e.g. [1] and refs therein). A previous parallelized 3D model [2] was based upon a mixed finite element/Fourier method, however, there were some limitations in the parallel algorithm and numerical routines. These limitations are removed in the new model presented here by using only transforms in Fourier space enabling more effective data organization across multiple parallel processors and therefore allowing larger, more complex FEL systems to be studied. Furthermore, unlike the previous 3D model, which uses commercial numerical packages, the new simulation code uses only open-source routines.

INTRODUCTION

As FEL's continue to push boundaries of radiation wavelength and pulse lengths, and with more complex FEL schemes to achieve these being explored, it may become necessary to extend the scope of what numerical FEL codes can model. Most current codes average the equations governing the FEL interaction over a radiation period and confine electrons to a localised region within one radiation period of their initial conditions (in the electron beam rest frame.) To describe the FEL interaction at the sub-radiation period scale, and to model electron migration over distances greater than the radiation period (non-localised), a numerical code that models the unaveraged equations governing the FEL interaction is required.

A 1D non-averaged model describing both sub-period phenomena and non-localised electron propagation has previously been developed [1, 3, 4]. More recently a 3D parallel non-averaged model for a helical undulator was developed in [2]. A substantially modified version of this 3D model, with significantly better parallel performance, is presented in this paper.

The 3D FEL model of [2] uses a split-step Fourier method [5]. This method separates a single numerical integration step, of the governing differential equations along the undulator, into two separate half-steps. In the first half step a Fourier transform method is used to solve for the field diffracting in the absence of any electron source terms. In the second half-step a Finite Element Galerkin Method [6] is used to solve for the field being driven by the electron sources, and in the absence of diffraction, while a 4th order Runge-Kutta method simultaneously drives the electrons. When parallelized using MPI, the model requires communication between three separate data sets distributed over multiple processors with each integration step of the code. The amount of communication between processors should be kept to a minimum if the run-time of a parallel code is to scale well with the number of processors used, otherwise the run-time benefit of using multiple processors can become significantly reduced [7].

The model presented here replaces the FEGM of the above model with a Fourier method (using open-source FFT routines [8]) similar to that described in [9]. The field is therefore now solved entirely in a 3D Fourier space. The method allows a reduction in communication between processors and gives a better scaling of the run-time benefit with increasing processor number. Furthermore, the commercial routines used for the FEGM are not needed, improving portability and allowing an open-source code when released.

The model is also generalised to allow any undulator polarisation from planar to helical, variable along the FEL interaction.

THEORETICAL MODEL

Starting from the 3D Maxwell wave equation and the Lorentz force equation, the 3D FEL equations for an helical undulator in the scaled dimensionless form of [2] may be written:

$$-i\rho\left(\frac{\partial^2 A}{\partial \bar{x}^2}+\frac{\partial^2 A}{\partial \bar{y}^2}\right)+\frac{\partial A}{\partial \bar{z}}+2i\rho\frac{\partial^2 A}{\partial \bar{z}\partial \bar{z}_2}=\frac{\gamma}{a_w \bar{n}_p}\times$$
$$\frac{\partial}{\partial \bar{z}_2}\sum_{j=1}^{N}\bar{p}_{\perp j}e^{i\bar{z}_2/2\rho}\sqrt{\frac{\epsilon Q_j(\epsilon Q_j+2)}{(1+|\bar{p}_{\perp j}|^2)}}\,\delta^3(\bar{x}_j,\bar{y}_j,\bar{z}_{2j}) \quad (1)$$

$$\frac{d\bar{p}_{\perp j}}{d\bar{z}}=\frac{a_w}{2\rho}\left[ie^{-\frac{i\bar{z}}{2\rho}}-\left(\frac{2\gamma_r\rho}{a_w}\right)^2\epsilon Q_j A e^{-\frac{i\bar{z}_{2j}}{2\rho}}\right]-$$
$$\frac{a_w^2\epsilon}{8\rho^2}\sqrt{\frac{Q_j(2+\epsilon Q_j)}{(1+|\bar{p}_{\perp j}|^2)}}\frac{(\bar{x}_j-i\bar{y}_j)}{(1+\epsilon Q_j)^2} \quad (2)$$

$$\frac{dQ_j}{d\bar{z}}=\frac{a_w}{4\rho}\frac{Q_j(\epsilon Q_j+2)}{1+|\bar{p}_{\perp j}|^2}\left[i(\epsilon Q_j+1)(\bar{p}^*_{\perp j}e^{-i\frac{\bar{z}}{2\rho}}-c.c.)+\right.$$
$$\left.\left(\frac{2\gamma_r\rho}{a_w}\right)^2\epsilon Q_j(\bar{p}^*_{\perp j}Ae^{-i\frac{\bar{z}_{2j}}{2\rho}}+c.c.)\right] \quad (3)$$

$$\frac{d\bar{z}_{2j}}{d\bar{z}}=Q_j \quad (4)$$

$$\frac{d\bar{x}_j}{d\bar{z}} = \sqrt{\frac{Q_j(\epsilon Q_j+2)}{1+|\bar{p}_{\perp j}|^2}}\mathrm{Re}(\bar{p}_{\perp j}) \tag{5}$$

$$\frac{d\bar{y}_j}{d\bar{z}} = -\sqrt{\frac{Q_j(\epsilon Q_j+2)}{1+|\bar{p}_{\perp j}|^2}}\mathrm{Im}(\bar{p}_{\perp j}) \tag{6}$$

where $\delta^3(\bar{x}_j,\bar{y}_j,\bar{z}_{2j}) \equiv \delta(\bar{x}-\bar{x}_j)\delta(\bar{y}-\bar{y}_j)\delta(\bar{z}_2-\bar{z}_{2j})$ and all variables are as defined in [2]. The only approximations made are the neglect of space charge, the paraxial approximation, and

$$\left|\frac{\partial E_\perp}{\partial \bar{z}}\right| << \left|\frac{\bar{\beta}_z}{1-\bar{\beta}_z}\frac{\partial E_\perp}{\partial \bar{z}_2}\right|,$$

where $E_\perp = \xi_0 e^{-i\frac{\bar{z}_2}{2\rho}}$ and $\xi_0(\bar{z},\bar{z}_2)$ is the complex radiation envelope. The latter approximation is made in [10] where, expressed in the independent variables $(\bar{z},\bar{z}_1)$, it is shown to be equivalent to the neglect of any backward propagating field. Focussing of the electron beam is described by the final term of (2) corresponding to the 'natural focussing' of an helical wiggler. This term is easily modified for other focussing systems.

The field equation (1) is solved using the Fourier split-step method by seperating it into diffraction-only and source-only parts. For diffraction only in the absence of sources the field equation is

$$-i\rho\left(\frac{\partial^2 A}{\partial \bar{x}^2}+\frac{\partial^2 A}{\partial \bar{y}^2}\right)+\frac{\partial A}{\partial \bar{z}}+2i\rho\frac{\partial^2 A}{\partial \bar{z}\partial \bar{z}_2}=0 \tag{7}$$

Defining the 3D Fourier transform

$$\tilde{A}(k_{\bar{x}},k_{\bar{y}},k_{\bar{z}_2},\bar{z}) = FT\left\{A(\bar{x},\bar{y},\bar{z}_2,\bar{z}\right\} \tag{8}$$

and applying to (7) yields the solution

$$\tilde{A}(\bar{z}_0+\Delta\bar{z}) = \tilde{A}(\bar{z}_0)\exp\left(\frac{-i\rho(k_{\bar{x}}^2+k_{\bar{y}}^2)}{1-2\rho k_{\bar{z}_2}}\Delta\bar{z}\right) \tag{9}$$

for an arbitrary initial $\bar{z}_0$ and where the dependence of $\tilde{A}$ on $(k_{\bar{x}},k_{\bar{y}},k_{\bar{z}_2})$ is understood.

In the absence of diffraction, but with electron source terms, the field equation becomes

$$\frac{\partial A}{\partial \bar{z}} = \frac{\gamma_r}{a_w\bar{n}_p}\sum_{j=1}^{N}\bar{p}_{\perp j}e^{i\bar{z}_2/2\rho}\sqrt{\frac{\epsilon Q_j(\epsilon Q_j+2)}{1+|\bar{p}_{\perp j}|^2}}\delta^3(\bar{x}_j,\bar{y}_j,\bar{z}_{2j}). \tag{10}$$

In the previous code of [2], the field equation (10) was solved simultaneously with the electron equations using a 4th order Runge-Kutta and FEGM. One integration step required 3 different sets of field data distributed across the parallel processors: one for the Fourier transforms used in the diffraction step, one for the finite element, and one for the RHS of the source equation (10) plus the electron equations. The optimum form of the electron data distribution also changes as they migrate across field elements.

The alternative solution presented here utilises a Fourier description of the field source term, similar to the multi-frequency FEL model of [9], so that the entire field equation may be solved in Fourier space. Fourier transforming (10) using (8) gives

$$\frac{\partial \tilde{A}}{\partial \bar{z}} = \frac{\gamma_r}{a_w\bar{n}_p}\sum_{j=1}^{N}\bar{p}_{\perp j}\sqrt{\frac{\epsilon Q_j(\epsilon Q_j+2)}{1+|\bar{p}_{\perp j}|^2}}\times$$
$$\exp\left[-i(k_{\bar{x}}\bar{x}_j+k_{\bar{y}}\bar{y}_j+\bar{z}_{2j}(k_{\bar{z}_2}-\frac{1}{2\rho}))\right] \tag{11}$$

Equation (11) describes how the electrons drive the field in 3D Fourier space and is relatively simple to solve numerically. To obtain the field in real space, required for the electron dynamic equations of (2...6), the inverse transform is all that is required and a finite element description of the field in real space is unnecessary.

VARIABLE UNDULATOR POLARISATION

The general form of the radiation field definition and the equation describing its evolution allows any field polarisation to be modelled. A relatively simple modification to the undulator field then allows modelling of an elliptically polarised FEL. The transverse terms of the magnetic wiggler field are re-defined as:

$$\mathbf{B_w} = \frac{B_w}{\sqrt{2}}(\mathbf{f}e^{-i\frac{\bar{z}}{2\rho}}+c.c.), \tag{12}$$

where the new basis vector $\mathbf{f} = (H\hat{\mathbf{x}}+i\hat{\mathbf{y}})/\sqrt{2}$ and the constant H has limits $0 \le H \le 1$, where $H=1$ corresponds to an helical undulator and $H=0$ for a planar undulator. For simplicity here, the axial terms of the wiggler field that give the natural focussing remain unchanged from [2]. Note that $\mathbf{f}$ is not a unit vector and the scaling of the equations is with respect to the y-component of the undulator magnetic field. The scaling factor H appears explicitly in the equation of motion for $\bar{p}_{\perp j}$ only:

$$\frac{d\bar{p}_{\perp j}}{d\bar{z}} = \frac{a_w}{2\rho}\left[\frac{i}{2}\left((1+H)e^{-\frac{i\bar{z}}{2\rho}}-(1-H)e^{\frac{i\bar{z}}{2\rho}}\right)-\right.$$
$$\left.\left(\frac{2\gamma_r\rho}{a_w}\right)^2\epsilon Q_j A e^{-\frac{i\bar{z}_{2j}}{2\rho}}\right]-$$
$$\frac{a_w^2\epsilon}{8\rho^2}\sqrt{\frac{Q_j(2+\epsilon Q_j)}{(1+|\bar{p}_{\perp j}|^2)}}\frac{(\bar{x}_j-i\bar{y}_j)}{(1+\epsilon Q_j)^2} \tag{13}$$

with all other equations in (1...6) remaining unchanged. Note that this form allows the undulator polarisation factor to vary as a function along its length $H(\bar{z})$.

NUMERICAL MODEL

The summation over real electrons is changed to a summation over macro-particles using the method of [1]. The localised electron density over a volume element $\bar{V}_k$ in the scaled space $(\bar{x}, \bar{y}, \bar{z}_2)$ containing N_k electrons may be described as a by a fractional weighting factor $0 < \chi_k \leq 1$ of the scaled peak electron density in the pulse:

$$\frac{N_k}{\bar{V}_k} = \chi_k \bar{n}_p. \tag{14}$$

Using (14), the sum over N real electrons, appearing in the source term of (11), changes to a sum over $k = 1 \ldots N_m$ macroparticles each of electron charge weight N_k as follows:

$$\frac{1}{\bar{n}_p}\sum_{j=1}^{N}(\cdots)_j = \frac{1}{\bar{n}_p}\sum_{k=1}^{N_m} N_k(\cdots)_k = \sum_{k=1}^{N_m}\chi_k \bar{V}_k(\cdots)_k \tag{15}$$

Defining the normalized weighting $\bar{\chi}_k = \chi_k \bar{V}_k$, the final form of the Fourier field equation (11) implemented in the code is obtained:

$$\frac{\partial \tilde{A}}{\partial \bar{z}} = \frac{\gamma_r}{a_w}\sum_{k=1}^{N_m}\bar{\chi}_k \bar{p}_{\perp k}\sqrt{\frac{\epsilon Q_k(\epsilon Q_k + 2)}{1 + |\bar{p}_{\perp k}|^2}} \times$$
$$\exp\left[-i(k_{\bar{x}}\bar{x}_k + k_{\bar{y}}\bar{y}_k + \bar{z}_{2k}(k_{\bar{z}_2} - \frac{1}{2\rho}))\right]. \tag{16}$$

The Fourier field is discretized into nodes along each axis $(\bar{x}, \bar{y}, \bar{z}_2)$ and wavevector k-values take the general form $k = 2\pi n/l$, where the integer $-M/2 \leq n \leq M/2$ and M is the number of nodes spanning length l along the axis. The numerical fast-Fourier transforms are taken using the parallel processor FFTW open-source package [8]. The macroparticles and fourier field nodes are initially distributed uniformly among the parallel processors with increasing $\bar{z}_2$.

The new split-step Fourier method consists of the following steps:

1. Field Diffraction Step: The Fourier field diffraction equation (9) is solved. Data redistribution of the transformed field is not required.

2. Field Driving and Electron Propagation Step: The Fourier field source equation (16) is solved and the macroparticle equations (2-6) are propogated using a 4th order Runge-Kutta method. Some macroparticle data needs to be communicated between processors to act as the source for all the Fourier field nodes of (16). After the macroparticles drive the field in Fourier space a backwards Fourier transform is required to calculate the real field for the macroparticle equations (2-6). The macroparticle equations are solved in parallel without need for communication of field data between processors.

3. The latter two steps are repeated until the end of the integration.

A summary of the differences between the previous FEGM algorithm of [2] and the new method presented here is shown in Fig. 1.

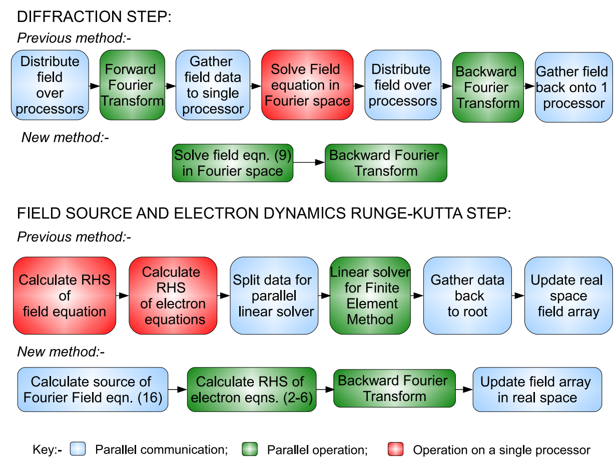

Figure 1: A schematic of the parallel algorithms showing the differences between the previous Finite Element Galerkin Method of [2] with the Fourier method presented here.

PLANE WAVE APPROXIMATION

The field description can be altered to approximate a plane wave by using only one node in the tranverse plane. Only the constant, non-oscilatory term of the numerical Fourier series then exists i.e. $k_{\bar{x}}, k_{\bar{y}} = 0$ and the field is then only a function of $\bar{z}_2$. Note, however, that this plane wave representation of the field still allows full 3D electron dynamic effects such as emittance and beam focussing to be modelled correctly. For a 'full' 1D limit, only one macroparticle, and so one value of the transverse variables, is used for each position in $\bar{z}_2$. The model is therefore quite flexible enabling a range of effects to be modelled, from a relatively fast full 1D model, to the plane wave approximation while retaining complete 3D electron dynamics, to the complete 3D model for both radiation field and electron dynamics.

To make the plane wave approximation in the numerical model the real-space field equation (10) is first integrated over the transverse plane ($\bar{x}$,$\bar{y}$). The equation is then Fourier transformed to give:

$$\frac{\partial \tilde{A}}{\partial \bar{z}} = \frac{\gamma_r}{a_w}\sum_{k=1}^{N_m}\bar{\chi}_k^{(1D)}\bar{p}_{\perp k}\sqrt{\frac{\epsilon Q_k(\epsilon Q_k + 2)}{1 + |\bar{p}_{\perp k}|^2}} \times$$
$$\exp(-i\bar{z}_{2k}(k_{\bar{z}_2} - \frac{1}{2\rho})) \tag{17}$$

where $\bar{\chi}_k^{(1D)} = \chi_k l_k$ and l_k is the range of $\bar{z}_2$ initially occupied by the kth macroparticle. Simulations using the code in the full 1D limit give very good agreement with results from [1] and [3].

EXAMPLE

A simple example is used to demonstrate first simulation results using the code. Several high gain FEL schemes operating at short wavelengths propose to use the exhaust

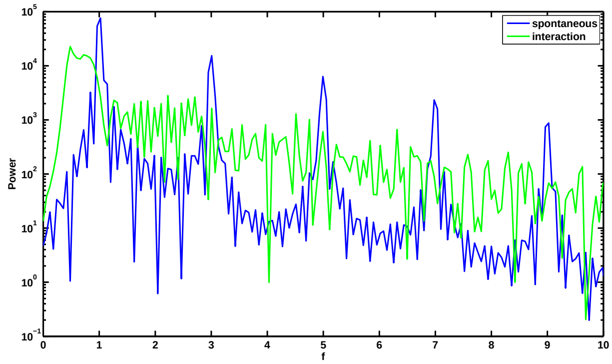

Figure 2: Spectra in the 1D planar wiggler limit for a short electron pulse generating CSR both with (green) and without (blue) coupling to the radiation field.

electron bunches to generate long wavelength radiation via Coherent Spontaneous Radiation, where the electron bunch length is less than the resonant wavelength of a long period undulator. While averaged FEL codes cannot model this interaction the non-averaged code described here can. Parameters similar to that of the UK NLS proposal [11] are used which in the scaling here are: $\rho \approx 0.24$; $a_w \approx 60$ and with a gaussian electron pulse $\sigma \approx 1/50$th that of a resonant radiation wavelength of $\lambda \approx 100\mu$m. The code simulated a planar undulator with $H = 0$ and operating in the 1D mode over 10 undulator periods (without any waveguide) of $\lambda_w = 1$m generates the spectra of Fig. 2 both with and without electron coupling to the radiation field. It can be seen that with electron coupling (green), the electron energy loss to the field shifts the resonant wavelength to longer wavelengths and significantly changes the spectrum from that of the uncoupled case (blue) which shows the usual CSR wiggler spectrum with odd harmonics clearly visible.

Using the same parameters, the second simulation demonstrates the code operating in 3D again with a planar wiggler. The scaled field polarisation is plotted in the $(\bar{x}, \bar{y})$ plane in Fig. 3 as a vector field. This polarisation does not change as a function of $\bar{z}_2$ so that it describes linearly polarised radiation and demonstrates the ability of the code to model variable polarisations.

CONCLUSION

A parallel FEL simulation code able to model sub-radiation wavelength effects and non-localised electron dynamics has been developed. This code algorithm significantly reduces run-time from the previous version of [2]. More rigorous testing and benchmarking of the code will be undertaken before release.

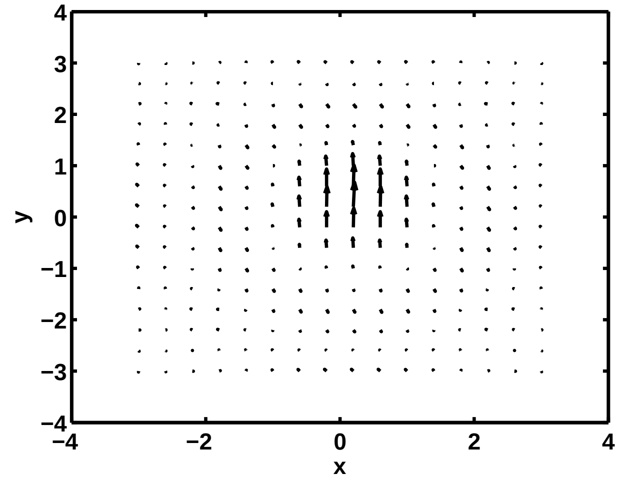

Figure 3: Scaled electric field vector plot using the code in the 3D planar wiggler limit to demonstrate generation of lineraly polarised radiation from a planar wiggler.

REFERENCES

[1] B.W.J. McNeil, M.W. Poole and G.R.M. Robb, Phys. Rev. ST Accel. Beams **6**, 070701 (2003); B. W. J. McNeil, G. R. M. Robb and M. W. Poole, MPPB060, Proceedings of the 2003 Particle Accelerator Conference, Portland, Oregon, USA (2003)

[2] C.K.W. Nam, P. Aitken and B.W.J. McNeil, MOPPH025, Proceedings of the 30th International FEL Conference, Gyeongju, Korea (2008); C.K.W. Nam, *On the Theory and Modelling of the Fourth Generation Light Source*, Ph.D. Thesis, University of Strathclyde (2009)

[3] B.W.J. McNeil, G.R.M. Robb and D.A. Jaroszynski, Opt. Commun. **165**, 65 (1999)

[4] B.W.J. McNeil, G.R.M. Robb and D.A. Jaroszynski, Nucl. Instrum. Methods Phys. Res., Sect. A **445**, 72 (2000)

[5] R.H. Hardin and F.D. Tappert, SIAM Review **15**, 423 (1973)

[6] K.H. Huebner E.A. Thornton and T.G. Byrom, *The Finite Element Method For Engineers*, Wiley (1995)

[7] P.S. Pacheco, *Parallel Programming with MPI*, Morgan Kaufmann Publishers, Inc. (1997)

[8] M. Frigo and S.G. Johnson, *FFTW 2.1.5 Manual* (2003) available from `http://www.fftw.org/`

[9] N. Piovella, Physics of Plasmas **6**, 3358 (1999)

[10] B.W.J. McNeil and G.R.M. Robb, Phys. Rev. E **65**, 046503 (2002)

[11] New Light Source (NLS) Project: Science Case and Outline Facility Design, Eds. J. Marangos, R. Walker and G. Diakun (2009) available from `http://www.newlightsource.org/`